Sorbonne University

M1 Internship - CompMech - 2020/2021

Optimal dynamical stabilization : application to an inverted electromagnetic pendulum

Author :
Valentin Duvivier
valentin.duvivier@etu.sorbonne-universite.fr

Supervisors :
Arnaud Lazarus
Suzie Protière

PhD student :
Alvaro A. Grandi

August 30, 2021

Contents

Abstract

My name is Valentin DUVIVIER and to validate my master 1 Computational Mechanics, I have done the internship *"Optimal dynamical stabilization : application to the inverted electromagnetic pendulum"*. It took place at ∂'Alembert laboratory, directed by Pierre-Yves LAGREE.

My direct supervisors were Professor Arnaud LAZARUS and Researcher Suzie PROTIERE, as well as the PhD student Alvaro A. GRANDI. I therefore take these few lines to thank them for their help on choosing the system components, on their help with data post-process code, and on their overall help on experimental subjects, oral presentation and report construction.

Introduction

To study a system's dynamical behavior is a straightforward way to conclude on its stability. What is not so straightforward is how one can create dynamic stability in a system. As part of my Master 1 internship, I have for mission to proceed to the passive dynamic stabilisation of an upwards pendulum (i.e. inverted pendulum).

In detail, a pendulum has two static equilibriums : one that minimizes the energy and which is stable (simple pendulum), and another one that doesn't and which is unstable (inverted pendulum). We will then study the case of the inverted pendulum and seek a way to dynamically stabilize it.

The physicist Pyotr KAPITZA has already studied the stabilization of an inverted pendulum (IP) with a passive approach, modulating his system through a vertically vibrating pivot. KAPITZA's inverted pendulum had a fast driving frequency compared to the collapsing time, which implied the pendulum had to be quasi-constantly stimulated to remain stable upwards [1, 2].

On our side, we want to extend the study to the cases where the driving frequency is of same order than the collapsing time. In fact, if one considers KAPITZA had to quasi-constantly provide energy to the IP to make it hold, on our side we would like to optimize this energy, namely minimize it. To this aim, we will modulate the dynamic stability through an electro-magnet.

In practical terms, we will translate what is naturally an unstable system into a stable one by altering the effective gravity g_{eff} the mass is subject to. To do so, we use an electro-magnet which will create a magnetic field opposed to the gravity one and that one will be able to modulate through the current provided to it.

My work will be an exploration of the same order than the one Alvaro A. GRANDI did on a simple pendulum [3], expanded to the case of an inverted pendulum.

In a first time, we will proceed to the characterization of our system's behavior. We will first define the static stability of the IP before we head towards dynamic motion. The point will be to understand our system's motions and to eventually deduce a framework

where one can study dynamic stability.

In a second time, we will seek dynamic stability states. We will observe experimental dynamic stability and subsequently deduce a theoretical model for dynamic stabilisation.

We will conclude on the report results regarding IP's dynamical stabilisation and a discussion on the some field application.

1. Characterisation

In this chapter we give a thorough description of our system, detailing the components and method we used to study its static and dynamic motions.

1.1 Presentation system - Static stability

This section will be the place to do an overview of the system and go through the static stability.

1.1.1 Physical system

First and foremost, let's do an overview of the elements composing the system :

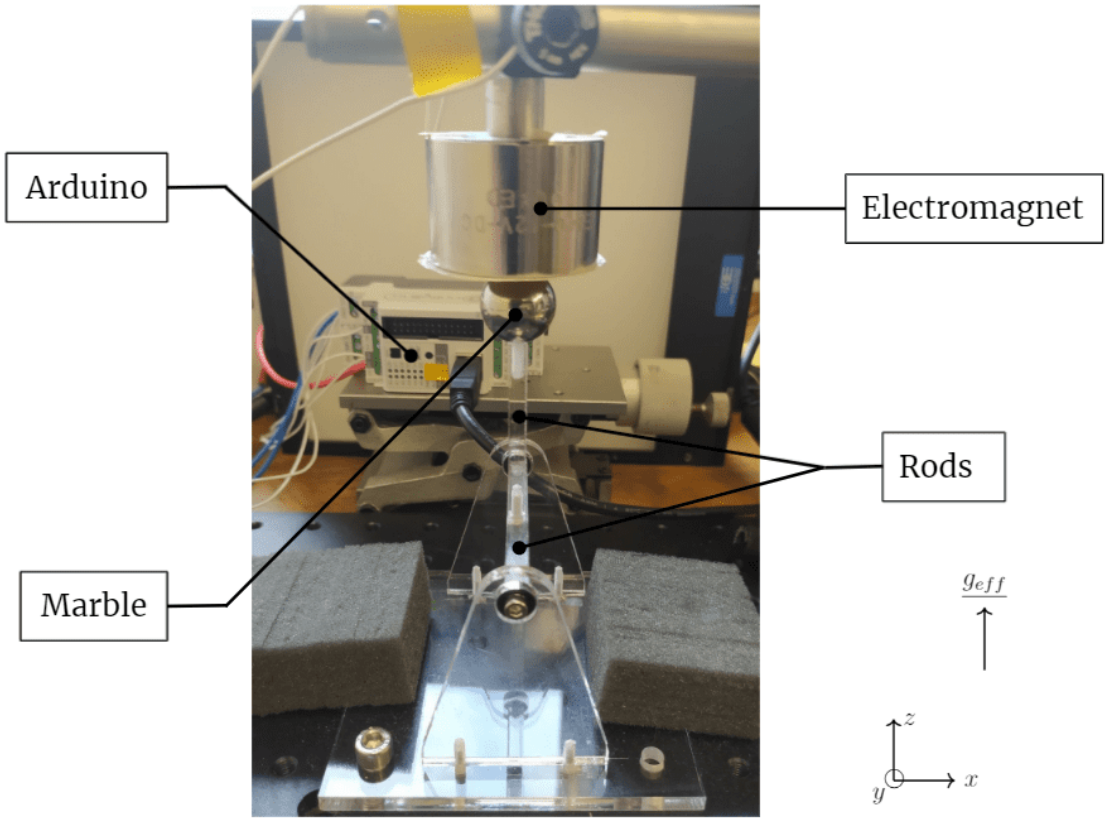

Figure 1.1: Photography of the inverted pendulum system

On above image, we can see the inverted pendulum (IP) holds in vertical position by use of an **electro-magnet** powered by a **battery** (out of frame here). The IP is here in its static equilibrium state.

Moreover, what we call IP is here a set composed of a spherical **marble** and 2 **rods**: one that holds the marble in place and another one around which rotation takes place.

We will see during dynamic phase that we transmit informations to the electro-magnet thanks to an **Arduino Controllino Mini** card.

To these main components, we add the following characteristic data :

- electro-magnet's radius $\rightarrow r_m = 20\text{mm} \pm 0.2\text{mm}$;
- marble's radius $\rightarrow r_b = 9.5\text{mm} \pm 0.2\text{mm}$;
- rod's length $\rightarrow L = 5.2\text{cm} \pm 0.2\text{mm}$;
- thickness/width of the rod $\rightarrow e = l = 5\text{mm} \pm 0.2\text{mm}$;

Given the materials associated to each of these elements, we finally obtain :

- marble's mass $\rightarrow M = 27.36\text{g} \pm 0.01\text{g}$;
- rod's mass $\rightarrow m = 1.53\text{g} \pm 0.14\text{g}$; *

* detail of the calculation is to be found in Appendix A - Relative error calculation.

This set of data defines our system. It implies that when we will later characterize our system, the gathered data will have to be accounted for this specific framework, namely they may vary slightly for another rod length, ratio marble/magnet, etc.

Let's now introduce an equivalent model from which we will work for the upcoming calculations.

1.1.2 Equivalent model

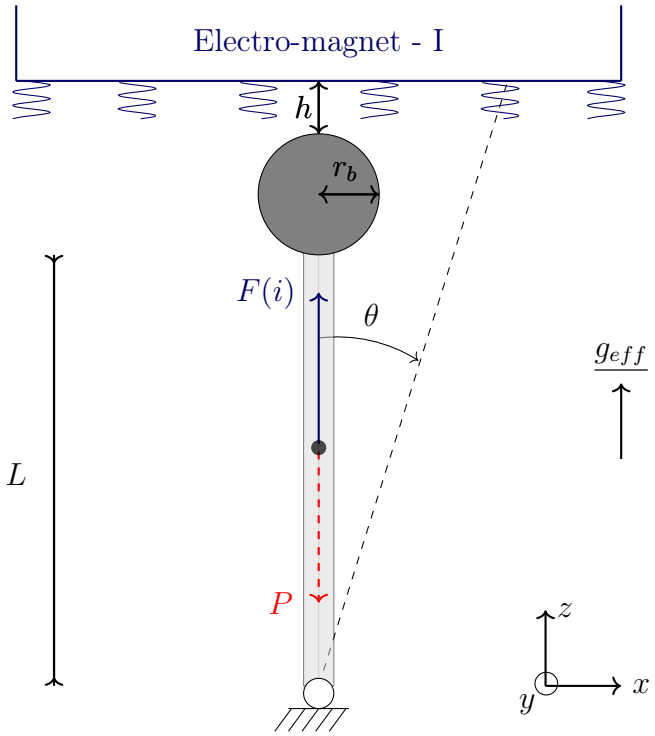

Figure 1.2: Model of IP system

In figure (1.2), the electro-magnet is turned ON and its attraction force is denoted $F(i)$. Given the IP remains stable in this vertical position, it's that $g_{eff} > 0$ and so $F(i) > P$ with P the IP's gravity force.

Let's furthermore define what it implies to go from an unstable to a stable system :

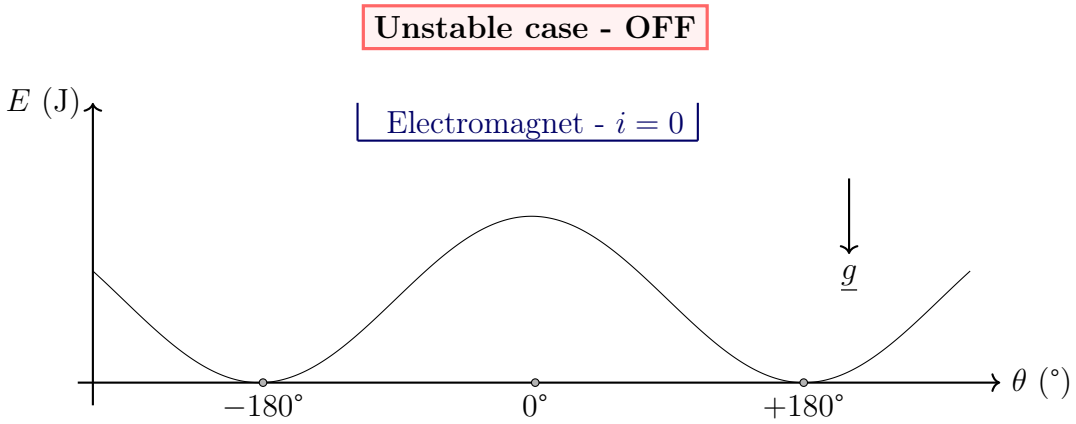

Figure 1.3: Illustration inverted pendulum's potential energy well

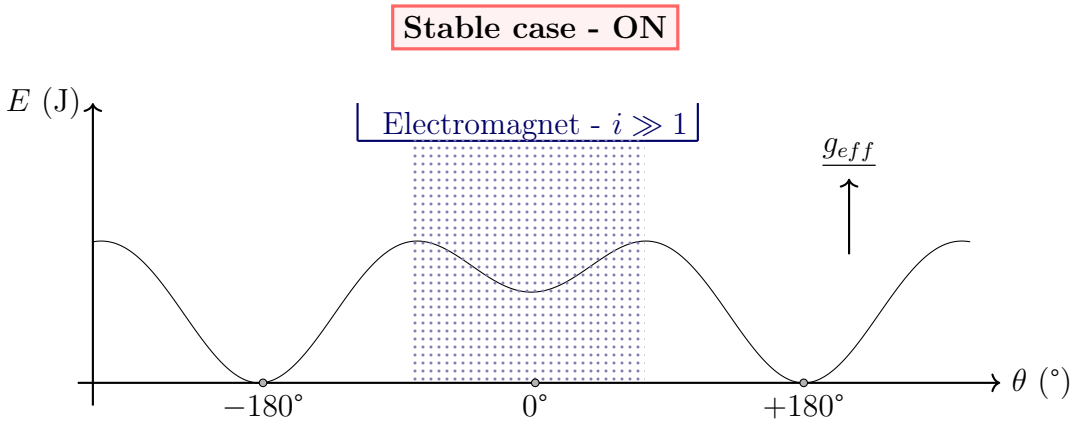

Figure 1.4: Illustration stabilized inverted pendulum's potential energy well

These graphs both show the state where pendulum is in vertical position, in the case where electro-magnet in turned OFF (1.3), and in the case where it's turned ON with $g_{eff} > 0$ (1.4).

Indeed, when the electro-magnet is OFF, we are in the usual case of gravity field. Yet, when we put electro-magnet ON, for a current high enough, we hold IP upwards. Then the more current we provide, the more the IP holds in this position. Physically, this translates into an upward effective gravity, modulated through the current i. In terms of energy, we created a new energy well by use of the electromagnet where the IP now is stable.

The next step will be to characterize the system's static and dynamic states. To do so we introduce 3 parameters : the distance marble/electro-magnet h, the angle θ and the current i. The purpose will be to define domains for each of these variable.

To begin with, we must describe how we define static stability.

1.1.3 Static stability - Magnetic field's homogeneity

We understand the physical limits of our system by understanding the link between a stable IP and the current i needed to sustain it. The point is that the current is the parameter that modulates the magnetic force, and so the effective gravity. We then expect to be more stable when the current ($\equiv$ the magnetic force) is greater.

We then want to know the minimum current (i_s) one needs to give to the IP in order to maintain it straight, as a function of the distance between the marble and the magnet (h). Besides, we test the magnetic field's homogeneity.

After experimental measurements we get the following graph :

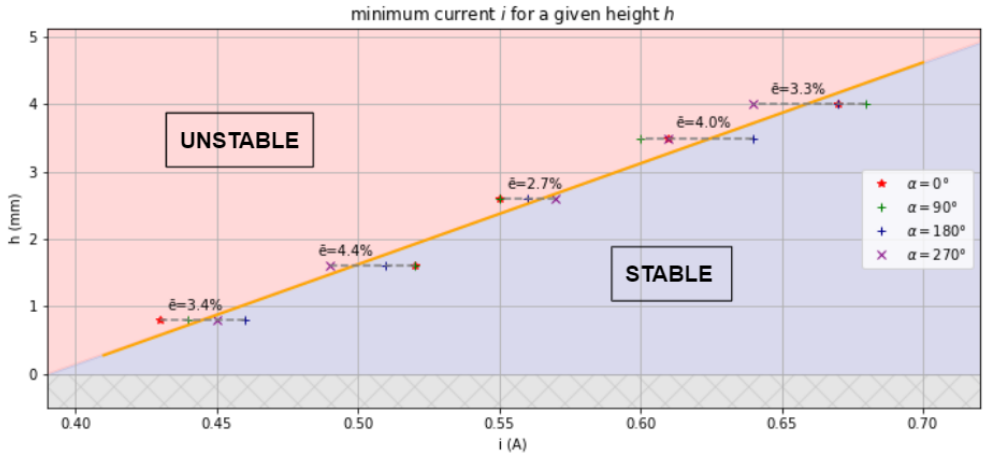

Figure 1.5: static stability zones in function of the current i and distance h

This graph represents the zone where IP is statically stable. Given a couple (h, i), one knows if the IP will remain stable or not.

Graph (1.5) is made of 20 experimental values : we seek i_s for 5 different heights, and we test homogeneity through 4 positions below magnet. We thus map magnetic field through 4 points only to then extrapolate to the whole field. Note that we should have i_s constant at a given height, and we check if it's the case.
Then the error measures this difference : it's the relative error from point farther from mean line to mean line (max relative error at given height).

Moreover, we decided to do a linear numerical interpolation (orange line) given the alignment of experimental points. In the end we have an empirical model (orange line) that will provide a link between h and i_s.

For instance, the graph allows to see that for $h \to 0$, $i_s \neq 0$. Indeed, i_s is the current at which IP holds straight, and as our system is unstable, we can't have $i_s = 0$ where IP remains straight on its own (not in a stable way). It confirms the physical reliability of this graph.

Besides, at fixed height, we have an associated i_s, but one can vary i from i_s to ∞. We can work everywhere at orange line's right to have straight IP at rest (i.e. continuous current). We will later see why we decided to fix $h = 0.6$mm and $i = 0.48$A, then reducing the number of parameters we deal with.

Now that the static state is understood, we will introduce the dynamic motion, namely when the electro-magnet is turned ON and OFF for a long time.

1.2 Dynamic motion - ON and OFF behaviors

To tackle the pendulum's dynamical behavior, we study IP's motion when electro-magnet is OFF or ON. Then, knowing behavior at these states one will be able to combine them in a second time to look for dynamic stability.

This section will then be decomposed into two subsections :

- one on damped vibrating behavior - ON ($i > i_s$);
- another one on falling behavior - OFF (i=0A).

Let's first derive the equation of an inverted pendulum to see how we will adapt it to our 2 phases. We will then use Lagrange formula to go from energies and forces defining our problem to a motion equation.

We point out that as current i is one of our modulation parameters, some of our variables will depend on it, as the electro-magnetic force $F(i)$. On the contrary, under the assumption of a homogeneous magnetic field, we consider these variables, for instance F, such that $\frac{dF}{d\theta} = 0$, namely the electro-magnetic field is homogeneous beneath magnet. The point will then be to determine where it's physically the case :

$$\frac{d}{dt}\left(\frac{\partial L}{\partial \dot{q}}\right) - \frac{\partial L}{\partial q} + \frac{\partial D}{\partial \dot{q}} = Q$$

with $D = \frac{1}{2}C\dot{\theta}^2$ the friction term, Q the term of generalized forces, and L the Lagrangian, with $L = T - U$, T the kinetic energy and U the potential energy.

By application of Lagrange formula :

$$((M+m)||\underline{OG}||^2 + I_{Gy}).\ddot{\theta} + C(i).\dot{\theta} + (F(i) - (M+m)g) \times ||\underline{OG}||.sin(\theta) = 0$$

Then in linear theory ($\theta \ll 1$) under canonical form :

$$\Rightarrow \ddot{\theta} + 2\xi(i)\omega(i)\dot{\theta} + \omega^2(i)\theta = 0 \tag{1.1}$$

with $\omega(i)$ the vibration frequency and $\xi(i)$ the damping factor. They both depend on parameter i through $C = C(i)$ and $F = F(i)$. See Appendix A - Oscillation equation for

the complete expression of each of above terms.

Applying some elementary simplification :

$$\omega(i) = \sqrt{\frac{(F(i) \times ||\underline{OG}||}{((M+m)||\underline{OG}||^2 + I_{Gy})} - \frac{(M+m)g \times ||\underline{OG}||)}{((M+m)||\underline{OG}||^2 + I_{Gy})}} \approx \sqrt{\frac{F(i)}{ML^2} - \omega_0^2}$$

neglecting rod's mass and inertia around $\underline{e_y}$, namely $m \ll M$, $I_{Gy} \approx 0$ and $||\underline{OG}|| \approx L$.

Thereby $\omega_0^2 \approx \frac{Mg \times L}{ML^2} = \frac{g}{L}$ in this approximation and so :

$$\omega(i) \approx \sqrt{\frac{F(i)}{ML^2} - \omega_0^2} = \sqrt{\frac{1}{L}\left(\frac{F(i)}{M} - g\right)} = \sqrt{\frac{g_{eff}(i)}{L}}$$

with $g_{eff}(i) = \frac{F(i)}{M} - g$

We then know the sign of g_{eff} is directly bounded to the system's equilibrium :

- $g_{eff}(i) < 0$: we are back to the case of simple pendulum, then IP is unstable and falls;
- $g_{eff}(i) = 0$: forces are exactly balanced. This equilibrium is unstable given we are at the limit of stability (unstable equilibrium) ;
- $g_{eff}(i) > 0$: we are in a stable equilibrium where $F(i) > P$.

By modifying i, we change this effective gravity and so we have a direct impact on the system's stability. Let's now take a precise look at the two states ON ($g_{eff}(i) > 0$) and OFF ($g_{eff}(i) < 0$).

1.2.1 ON - $i > i_s$ - Damped vibrations

We proceed to experimental measures when electro-magnet is constantly ON : we offset IP from its equilibrium position, to then let it vibrate until totally damped due to friction. We want to confirm the motion during this phase is provided by equation (1.1) and deduce a domain where we can work at in term of angles and heights. Since i is the parameter we deal with, we will from now on work with fixed values of i instead of $g_{eff}(i)$.

The process is the following one :

- we want to determine the domain where θ is low enough to have a homogeneous field (e.g. $\frac{dF}{d\theta} = 0$). We thus test 3 impulses, each associated to a domain of angles: $\theta < 2°$, $2° \leq \theta \leq 6°$, $6° < \theta$;
- we test these impulses for several h to see their influence on homogeneity ;
- in the end we do video capture for 12 measures : 4 heights with 3 impulses each ;
- the post process will lead to values for the period T and the damping factor ξ ;
- we then compare experimental behavior to theoretical formula.

This so called theoretical formula is the solution to equation (1.1) which is :

$$\theta(t) = e^{-\omega\xi t} \times \left(cos(\omega_d t)\theta_0 + sin(\omega_d t) \times \left(\frac{\theta_0}{\sqrt{1-\xi^2}} + \frac{\dot{\theta}_0}{\omega_d} \right) \right) \tag{1.2}$$

with θ_0 the initial angle and $\dot{\theta}_0$ the initial angular speed of the IP, and $\omega_d = \omega \times \sqrt{1-\xi^2}$.

Let's now see the kind of comparison we want to do between experimentation and theory, before we develop the steps done to achieve it :

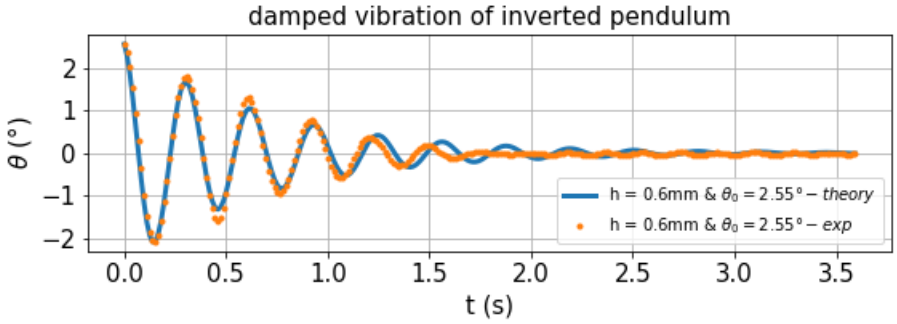

Figure 1.6: Superposition of experimental graph and optimized theory - case $h = 0.6$mm and $i = 0.48$A

First and foremost, we talk about comparison with theory in the sense that we get a couple $(\omega, \xi)_{exp}$ from experimentation (exp), and we implement it in our solution for damped vibration equation (1.2). Therefore, one should obtain two superposing curves but we didn't really fit theory at first and so we tried to think about this differently.

What we did was to look for an optimal couple $(\omega, \xi)_{opti}$ that would fit the best our experimental graph from the theoretical formula. Thus : if the tested point (h, θ_0) has a couple $(\omega, \xi)_{opti}$ that fits empirical data with theoretical equation (1.2), it's that this point respects homogeneity criterion. In a final comparison, we check that the values $(\omega, \xi)_{opti}$ are close to the one of $(\omega, \xi)_{exp}$. This whole process is based on the fact that there may be a solution to our problem with coefficients $(\omega, \xi)_{opti}$ close to the one we have $(\omega, \xi)_{exp}$. We then simply build a code that tests efficiently multiple couples, and so for each of our 12 points.

We decided to test a bunch of values of (ω, ξ) and to calculate the L2 norm relative error for each couple (h, θ_0). We here tested 10^2 values for ω and ξ, which implies 10^4 possible combination tested. We then sought the one that minimized the most the error, which was the one representing the optimal solution associated to our experimental graph.

We deduced the coordinates of this minimum point, to which was associated a couple $(\omega, \xi)_{opti}$.

It's at this stage that we obtained figure (1.6), which tells us that the point $h = 0.6$mm with $\theta_0 \approx 2.55°$ respects homogeneity given L_2 error is then minimized. However, while

all of the 12 points present a $L_{2_{min}}$, not all of them have $L_{2_{min}} \to 0$, where experimentation and theory fit the best (i.e. $L_{2_{min}} = 0$ is case where exp=theory). Thus, we know this method will limit the framework as expected.

From this process for each of the 12 couples, we deduce ranges $h \in [0.5;\ 2.0]$ mm and $\theta \in [2.0;\ 6.0]^\circ$ where the magnetic field is homogeneous.

One can work at any heights he wants except the bigger h, the least homogeneity is fulfilled. Thereby, we decide to remove h parameter from the problem by fixing $h = 0.6$mm, a height where we fulfill homogeneity. Yet from figure (1.5), we get $i_s \approx 0.43A$ such that at $h = 0.6$mm one can work at $i \in [0.43A, \infty[$.

At this stage, we are able to post process a video to get values of $(\omega,\ \xi)$ for given parameters $(h,\ i)$. As we removed h variable for simplification sake, we are left with a one parameter problem, provided homogeneity is fulfilled (namely no influence of θ on magnetic field's homogeneity then). Thus, to have some insight on the physic of our system, let's map $(\omega,\ \xi)$ values as functions of i for $h = 0.6$mm. Note that the same can be done for any h.

Extension to any current i

We proceed to the same post process than damped vibration phase section (1.2.1), which for a given i provides values for $(\omega,\ \xi)$. Testing a bunch of i, here is what we obtain :

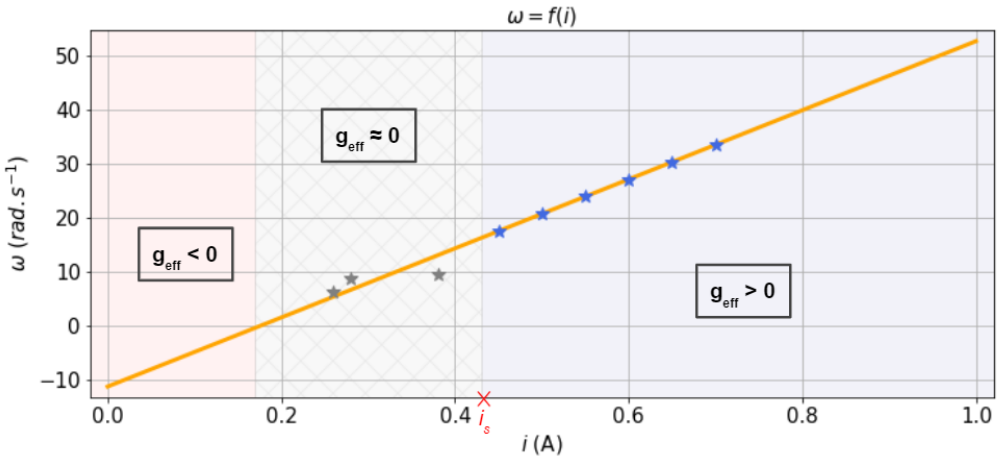

Figure 1.7: Mapping vibration frequency $\omega(i)$ for $h = 0.6$mm

One can see that to have mapped the vibration frequency ω as a function of i highlights a linear relation where bigger i, bigger $\omega(i)$. This graph has in fact been obtained by a linear numerical interpolation given the alignment of 6 experimental results (blue dots) at $i > i_s$. Thereby, the orange line once again represents an empirical model, from which one could for instance interpolate values of ω at low i.

$\omega(i)$ being proportional to electro-magnetic force $F(i)$, the bigger i, the bigger $F(i)$ and so the bigger $\omega(i)$, which explains the fact the vibration frequency increases with current i.

By association, the bigger $\omega(i)$, the bigger the effective gravity $g_{eff}(i)$ and so the more stable the system is.

Inversely, $\omega(i)$ becomes negative for i too low. These observations confirm the physical equivalence we did between system's vibration frequency $\omega(i)$ and effective gravity $g_{eff}(i)$. More precisely :

- $\omega = 0$ is when $F(i) \approx P$, which is at $i \approx 0.17$A. This limit in fact corresponds to the i_{min} below which IP falls (i.e. case $g_{eff}(i) = 0$) ;
- $\omega(i = 0)$ is the pulsation when $i = 0$A, which as we know is the natural growth rate, namely $\omega(i = 0) = -\omega_0 < 0$ (i.e. case $g_{eff}(i) = -g < 0$).

The grey dots represent experimental measurements at $i < i_s$, where IP isn't straight anymore. These points don't look as aligned as were the 6 previous ones. However, we confirm one can interpolate values of ω at low i, except it's difficult to observe it experimentally, given our system's likeliness to instability at low i.

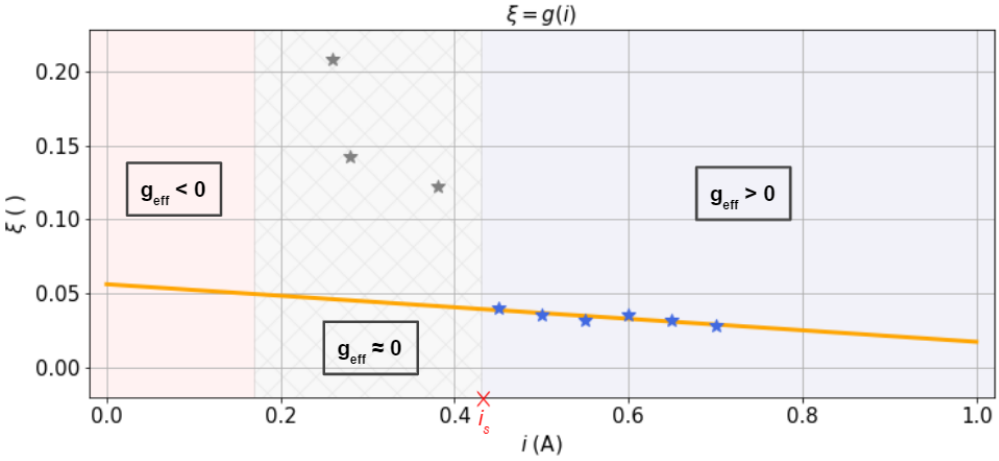

Figure 1.8: Mapping damping factor $\xi(i)$ for $h = 0.6$mm

The empirical model of damping factor $\xi(i)$ in figure (1.8) shows that it's a decreasing function of the current i. We furthermore see that we have very disparate value depending if we are either at $i > i_s$ (blue dots) or at $i < i_s$ (grey dots).

In fact, above graphs (1.7) and (1.8) gather two physics :

- one at $i < i_{min} \equiv g_{eff} < 0$ where IP collapses ;
- and another one at $i \geq i_{min} \equiv g_{eff} \geq 0$ where IP holds upwards ;

For instance, in the case of damping factor $\xi(i)$ we will get that once we are at $i < i_{min}$, we no longer have ξ increasing but rather $\xi(i) \approx 0$. A deeper look to the OFF state will then be needed to conclude on our empirical models (1.7) and (1.8).

1.2.2 OFF - $i = 0$A - Collapsing

In this section we go through the unstable aspect of our system : case where electromagnet is turned OFF. When we don't try to hold the IP up, we are back to the simple pendulum case. We study this phase in order to have more insight on the shape of collapsing, the natural growth rate ω_0, etc.

The equation describing motion is equation (1.1) with $i = 0$A, namely $F(i) = 0$ and $\xi(i) \approx 0$, so we get :

$$\ddot{\theta} - \omega_0^2 \theta = 0 \tag{1.3}$$

whose solution is

$$\theta(t) = cosh(\omega_0 t)\theta_0 + sinh(\omega_0 t)\frac{\dot{\theta}_0}{\omega_0} \tag{1.4}$$

This equation as well assumes linearity. Let's now describe the experimental process used to get $\omega_{0_{model}}$:

- we put IP as much at center as possible, namely $\theta \to 0°$;
- we then turn battery OFF and observe motion when falling ;
- finally we want to compare experimentation to theory and deduce $\omega_{0_{model}}$ using the same process than for the ON phase : fit experimental result with theoretical formula and deduce $\omega_{0_{model}}$. This value should be the same than the one of figure (1.7) for $\omega(i = 0A)$ as well as the one from theory $\omega_{0_{theo}} \approx \sqrt{\frac{g}{L}}$.

Let's now see the kind of comparison we obtained between experimentation and theory, before we develop the steps done to obtain it :

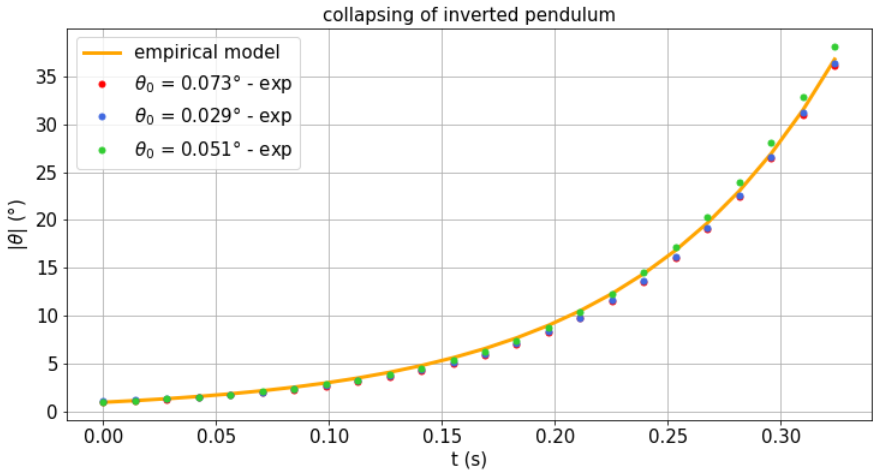

Figure 1.9: Collapsing behavior - empirical model vs experimentation

Before we reached graph (1.9), experimental data behaved as theory did but with an offset in time. It looked like this offset translated a paradox as well as it indicated the possible presence of friction :

- the more symmetric IP is, the more it holds into this position, until theoretically it doesn't move at all for $\theta = 0°$. The paradox lays in the fact that we must ensure symmetry to be reliable on angle's value, but if we are too much, we prevent motion;

- it may as well be that there is some friction slowing down the IP in addition to the symmetric influence. Then inertia makes it longer to have movement.

In the end, as we didn't know quantitatively the influence of friction, we decided to "force" movement to fit theory. It translated physically into an initial angle we gave to the IP to make it move sooner. The point was to not directly conclude on the system illness but to see if there existed a range of angles where exp and theory superposed.

We found after a few angle testing that $\theta = 1°$ was the limit angle above which theory and experimental graphs superposed. We then minimized the L_2 norm error between theory and experimentation, looking for $\omega_{0_{model}}$. The minimisation was made such that experimentation and theory fitted from $\theta = 1°$ to $\theta = 25°$ (i.e. value above which we are not linear anymore). The error minimisation process made, we reached a unique value of ω_{0model} that we used for the empirical model.
For comparison sake, we got that $\omega_{0_{model}} \approx 11.1\ rad.s^{-1}$ while $\sqrt{\frac{g}{L}} \approx 12.6\ rad.s^{-1}$

We can see the simplification $\omega_0 \approx \sqrt{\frac{g}{L}}$ introduced previously holds, within an error of approximately 12%, widely acceptable here. It as well is very close to the value from figure (1.7), confirming furthermore the empirical models' reliability.

Let's now summarize what data did this chapter bring us and conclude on our system's consistency.

1.2.3 Balance sheet model and framework

At this stage, we have a choice to make : do we continue working with this system? Previous phases gave us some insight on IP behavior in prevision for the dynamic stabilisation process but they as well provided a refined framework where to work at.

Then, it's at this stage that we decide that **the characterized framework is comfortable enough for us to work with** (in term of acceptable heights, angles).

Here below we summarize what our model is :

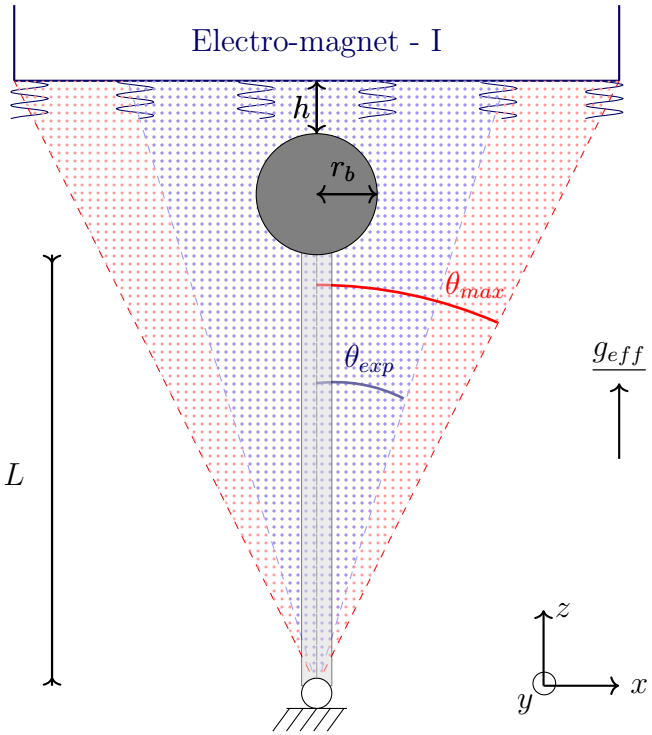

Figure 1.10: IP model's framework

Framework :

- we have a graph that says where to be at to ensure static equilibrium : figure (1.5) ;
- from the ON phase we decide to work at fixed height $h = 0.6$mm ;
- taking a physical step back, we have at $h = 0.6$mm :
  - $\theta_{max} \approx 10°$ above which marble isn't below magnet anymore ;
  - $\theta_{exp} \leq 6°$, range of angles where field's homogeneity is fulfilled.

With these informations in mind, let's see how it will translate when we combine ON and OFF motions.

2. Dynamic stabilisation - Energy optimization

The previous characterisation work settled the bases for dynamic behavior. We now know IP's behavior when the electro-magnet is respectively turned ON or OFF. Let's now combine these states in order to find stable dynamical equilibriums.

2.1 Stability modulation

For the moment, we know stability occurs when the electro-magnet is constantly ON, and that instability occurs when electro-magnet is OFF.

A mix of time ON (T_{ON}) and time OFF (T_{OFF}) will therefore be needed to work on dynamical stabilities, namely one may vary the ratio of time we are ON or OFF during one period.

Then, some couples (T_{ON}, T_{OFF}) will lead to stable behaviors while some others will lead to unstable ones. This in part defines the period of modulation $T = T_{ON} + T_{OFF}$.

Besides, to think in term of optimization one must consider the energy E as another parameter. To give a physical meaning to this chapter, we decide to work at $i = 0.48$A, then fixing $E_0 = R \times i^2 \times 1h$. Indeed :

- at $h = 0.6mm$, empirical model of figure (1.5) provides $i_s \approx 0.43A$, and so we ensure stability by imposing $i = i_s + 0.05$A ;
- the energy provided by the battery to the system is mostly transferred under Joule energy form ;
- in addition to previous point, our system follows Ohm law such that $P = R \times i^2$ and $E_0 = P \times 1h = R \times i^2 \times 1h \approx 5.35$ Wh (see Appendix B - Fig 2 - resistance calculation for R calculation).

The energy E_0 is the one we produce when the electro-magnet is constantly turned ON ; it's as well the one we try to minimize through dynamical stability.

Let's now see how stability modulation can be explained graphically:

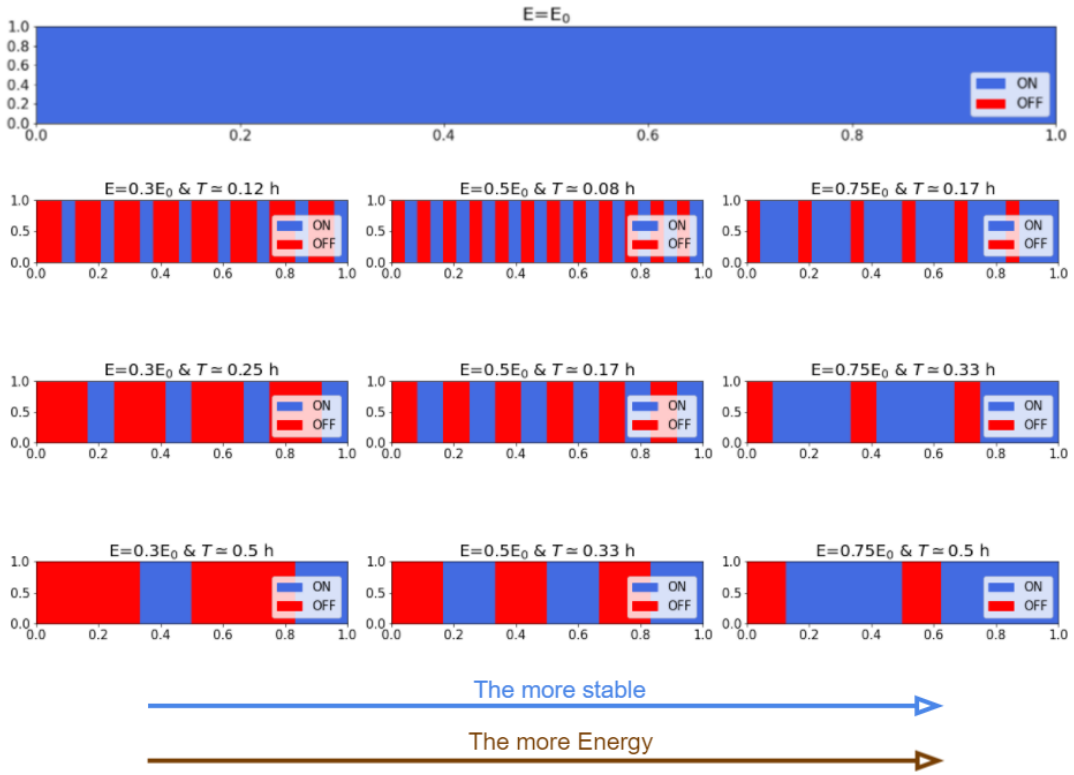

Figure 2.1: Experimental stability modulation under step function-like shape

While the first figure represents the case where we are constantly ON (i.e. we use $E_0 \approx 5.35$ Wh to make IP statically stable), the nine others are examples of couples of parameters (E, T) for dynamic motion.

In a first time, we want to find motions that minimize energy, and so we need to mix time ON and OFF, which are here respectively represented under blue and red surfaces. In fact, what tells us that energy is minimized is the ratio of colour :

- when blue, we use energy ;
- when red, we don't use energy ;
- $\Rightarrow$ the percentage of blue surface over a period of 1h indicates how much energy is used.

On figure (2.1), each column represents a certain energy minimisation. For instance, considering the third column, we have that one uses $E = 0.75E_0$. We thus use 75% of E_0 and so 75% of the period is in blue.

Similarly, when we are in the first column's case, we use $E = 0.30E_0$, so a use of 30% of E_0. Then, the blue surface represents 30% of the period while the red one represents the other 70%.

One can test any energy he wants, then reducing the initial energy E_0 used to make IP hold. However, not all cases represent stable motion. Here comes the time component.

As a matter of fact, once we set the ratio of colour, we can still split the 1h period as we wish. Considering the third column, we have three examples of how one can possibly allocate time. It's then possible to make fit any period that respects the forementioned energy ratio, namely here :

- Example : 3^{rd} column : case $E = 0.75E_0$
  - 1^{st} line : case where we have 6 periods in 1h ;
  - 2^{nd} line : case where we have 3 periods in 1h ;
  - 3^{rd} line : case where we have 2 periods in 1h ;

The point is that each of the 3 lines provides different values for (T_{ON}, T_{OFF}). Eventually, we have seen in these examples how one can use E and T as parameters to test different dynamic motions, which will result either on a stable or an unstable state, which only experimentation will tell.

With our two parameters in mind, let's now go through experimentation to see what dynamical behaviors we observe.

2.2 Experimental dynamic motion

Thanks to the results from chapter (1.2), we now have a protocol ready to apply to test oscillations:

- we put IP to straight position and hold it during 5s, thus avoiding motion as much as possible (through damping), namely $\theta \to 0°$;
- then an impulse is given to IP under the form of turning OFF IP during 250ms;
- afterwards we periodically turn the electro-magnet ON and OFF and observe its behavior.

The code associated to this protocol is transmitted using the Arduino Controllino mini card. As our system is passive, we transmit once at $t = 0s$ and see what occurs along time. We experimentally get :

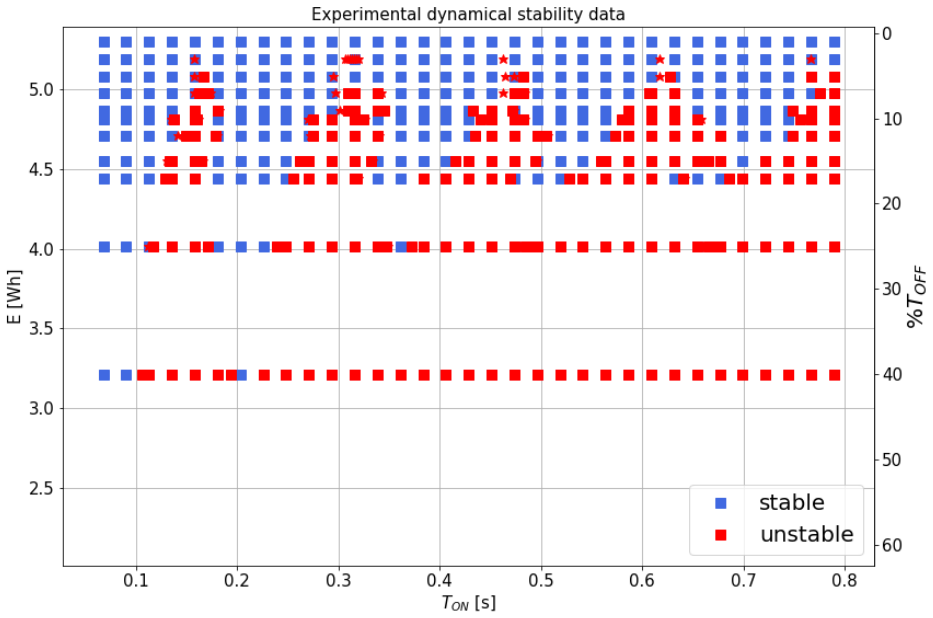

Figure 2.2: Experimental dynamical stability measures

Each of the above points is experimental and represents a state of the inverted pendulum (IP) after a long time ($\approx$ 30s). The two final states we observe are stable state (blue square) and unstable state (red square). Some of the states, represented by red stars are in fact non-damped oscillations which stemmed from the system's friction and dynamical damping, resulting in an in-between zone where the IP is at the edge of instability.

Anyway, the existence of the blue squares implies that we found stable dynamical motions. Moreover, we as well observe dynamic stabilities whose driving frequency is of same order than collapsing time. Indeed, you will see in the next section that the stable points at the left are the one associated to KAPITZA's pendulum, and so the one at the right are the one fulfilling condition over driving frequency.

Furthermore, the energy used to reach these stable states is as well reduced. Indeed, this graph is made such that each line is at a constant energy, and that the energy is the lowest at the bottom and the highest at the top. In fact, one can look at each line as a percentage of E_0 :

- when we are at $E = E_0$, the percentage of time OFF is 0% ;
- to reduce the energy we use, we must increase the time we turn OFF during a period ;
- when we are at $E = 0$Wh, the percentage of time OFF is 100% ;

By association to figure (2.1), we set energy by saying how much we turn OFF during one period (condition on E); and we then test different time allocation (condition on T_{ON}).

Before we post-process our data, let's take a physical step back on the experimental context :

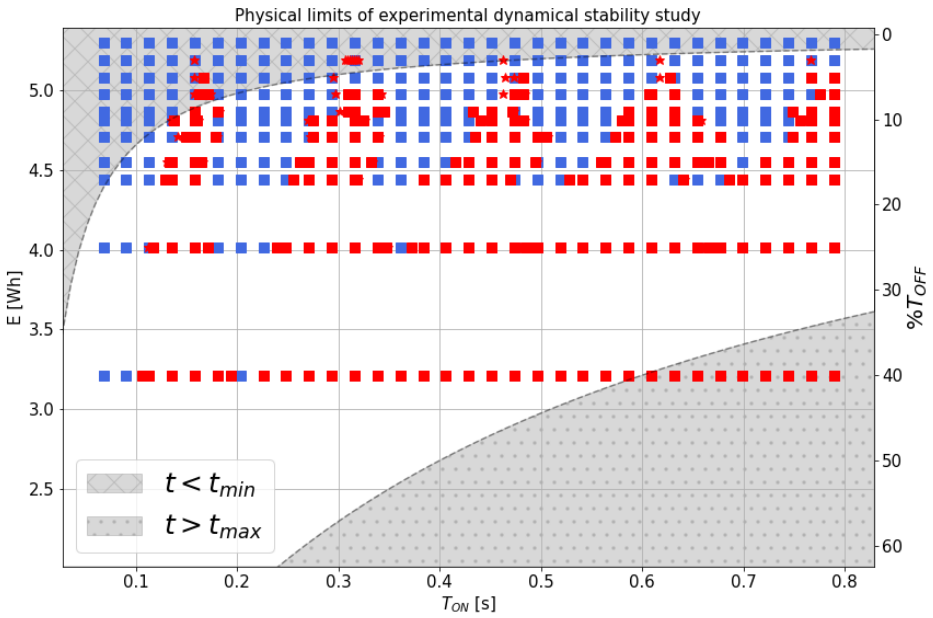

Figure 2.3: Physical limits of experimental measures

Quickly, we have two limitations :

- t_{min}, the time the battery takes to apply a change in current i ;
- t_{max}, the time above which the electro-magnet can't attract the marble anymore. It's at this time that $\theta = \theta_{max}$ 1.10.

To be on either of these grey zones may imply the experimental study isn't physically relevant.

Let's now post-process our experimental data. First, we see that we have more instabilities when E diminishes, namely with the percentage of time OFF increasing. Therefore, the more we're OFF ($\equiv$ the less we're ON), the more unstable the system is.

On the other hand, the stability doesn't only depend on E as we see on figure (2.2) that the system reacts differently depending on time T_{ON}. Note that we can equivalently consider T and T_{ON} as our modulation period, without any loss of generality.

We then observe 5 zones of instabilities that we will refer to as instability tongues. They look to appear at a characteristic time (periodic instability) and to extend with E decreasing. By association, we can see that the most one wants to minimize energy, the least dynamic stability exist (blue squares), until the dynamic stability exists in one point only.

In fact, these last existing dynamic stable points are the one optimizing the dynamic stability. From now on, we will then try to understand where they occur to conclude on the optimal dynamical stabilisation process.

Before going any further into the post-process, let's make sure our experimental data are relevant regarding dynamic stability. We thus decide to look at our system's theory. More precisely, we will see how Floquet theory can be used to derive an analytical theoretical solution and conclude on our experimental data relevance.

2.3 Floquet analytical theory

The usual method to test a system's stability is to give a little perturbation ϵ at an initial state and see how the system responds to it. Yet, our case is slightly more complex : we indeed deal with a periodic system that is ruled by 2 equations : (1.1) and (1.3).

A way to study stability then is to use Floquet theory that can provide informations on a solution's growth or decay along time. The point is to look at the solution's stability, without having to calculate it. We thus judge the evolution of the solution across time instead of looking at the solution itself.

We here recall the two motion equations (1.1) and (1.3) of dynamic behavior :

$$\begin{cases} \ddot{\theta} + & 2\xi(i)\omega(i)\dot{\theta} + \omega^2(i)\theta = 0 \\ \ddot{\theta} & - \omega_0^2\theta = 0 \end{cases}$$

We can combine these two equations into one considering we have time dependant factors $\omega(t)$ and $\xi(t)$. We thus have a periodic linear ordinary differential equation (ODE) on which one can apply Floquet theory. This periodic equation then is :

$$\ddot{\theta} + 2\xi(t)\omega(t)\dot{\theta} + \omega^2(t)\theta = 0 \tag{2.1}$$

which highlights the fact our coefficients are time dependent :

$$\omega^2(t) = \begin{cases} \omega^2(i) & \text{when ON} \\ -\omega_0^2(i) & \text{when OFF} \end{cases} \qquad \xi(t) = \begin{cases} \xi(i) & \text{when ON} \\ 0 & \text{when OFF} \end{cases}$$

Applying Floquet theory [4, 5], we know we will be able to rewrite this differential equation under a matrix form. To do so, let's consider $\underline{X}(t) = \begin{pmatrix} \theta \\ \dot{\theta} \end{pmatrix} \equiv \begin{pmatrix} x_1 \\ x_2 \end{pmatrix}$, then $\dot{\underline{X}}(t) = \begin{pmatrix} \dot{\theta} \\ \ddot{\theta} \end{pmatrix} = \begin{pmatrix} x_2 \\ -2\xi(t)\omega(t)x_2 - \omega^2(t)x_1 \end{pmatrix}$, such that an equivalent form of equation (2.1) is:

$$\{\dot{X}(t)\} = \begin{bmatrix} 0 & 1 \\ -\omega^2(t) & -2\xi(t)\omega(t) \end{bmatrix} . \{X(t)\} \tag{2.2}$$

We now want to see if this system is stable, namely if function $X(t)$ grows or decays along time. More precisely, one only has to look at behavior along one period given the system is T periodic, and so :

$$\{\dot{X}(t+T)\} = [A(t+T)] . \{X(t+T)\} \Rightarrow \{\dot{X}(t+T)\} = [A(t)] . \{X(t+T)\}$$

with $A(t) = \begin{bmatrix} 0 & 1 \\ -\omega^2(t) & -2\xi(t)\omega(t) \end{bmatrix}$

We then look at stability along 1 period to then extrapolate for all t. To work on system's stability, we introduce the existence of the monodromy matrix ϕ, which is at the heart of Floquet theory.

One of Floquet's theorem consists into comparing absolute values of Floquet multipliers λ_i with 1. Then :

- $|\lambda_i| > 1 \Rightarrow$ the solution is unstable ;
- $|\lambda_i| < 1 \Rightarrow$ the solution is stable ;

Yet, Floquet multipliers are the eigenvalues of the monodromy matrix ϕ. We thus look for this matrix to then run condition on it and deduce the stability state of the solution $X(t)$. However, as we have two states describing IP's motion (i.e. ON and OFF motions), we have two transfer matrices ϕ_1 and ϕ_2 that one will have to combine to get the monodromy matrix, namely :

$$\phi = \prod_{i=1}^{2} \phi_i$$

In a few steps :

- we transform system (2.2) into the equivalent one in the eigenvectors basis. Calling ϕ_i' the monodromy matrix in eigenvectors basis, we have $\phi_i' = e^{\Lambda T}$, with $\Lambda = \begin{bmatrix} \tau_1 & 0 \\ 0 & \tau_2 \end{bmatrix}$ [4,6] and $\tau_{1,2}$ the eigen values of matrix $A(t) = \begin{bmatrix} 0 & 1 \\ -\omega^2(t) & -2\xi(t)\omega(t) \end{bmatrix}$
- we go back to state space through $\phi_i = P\phi_i' P^{-1}$ with P the passage matrix and P^{-1} its inverse.
- eventually, to check solution's stability, we combine both solution according to the theorem $\phi = \prod_{i=1}^{2} \phi_i$ and look at Floquet multipliers ;

Eventually, one gets the following monodromy matrix, which is characteristic of pendulum-like systems :

$$\begin{aligned} \phi = & \frac{1}{\tau_2 - \tau_1} \begin{pmatrix} \tau_2 e^{\tau_1 T_1} - \tau_1 e^{\tau_2 T_1} & e^{\tau_2 T_1} - e^{\tau_1 T_1} \\ \tau_2 \tau_1 \left(e^{\tau_1 T_1} - e^{\tau_2 T_1} \right) & \tau_2 e^{\tau_2 T_1} - \tau_1 e^{\tau_1 T_1} \end{pmatrix} \times \\ & \frac{1}{\mu_2 - \mu_1} \begin{pmatrix} \mu_2 e^{\mu_1 T_2} - \mu_1 e^{\mu_2 T_2} & e^{\mu_2 T_2} - e^{\mu_1 T_2} \\ \mu_2 \mu_1 \left(e^{\mu_1 T_2} - e^{\mu_2 T_2} \right) & \mu_2 e^{\mu_2 T_2} - \mu_1 e^{\mu_1 T_2} \end{pmatrix} \end{aligned}$$

with $T_1 \equiv T_{ON}$, $T_2 \equiv T_{OFF}$; $\tau_{1,2}$ the eigen values of ON phase's system and $\mu_{1,2}$ the eigen values of OFF phase's system. Note that one can derive same result for the non-damped case system, considering $\xi(i) \approx 0$ when ON.

The monodromy matrix then leads to the Floquet multipliers through some properties:

$$\begin{aligned} & det(\phi) = 1 \Rightarrow \lambda_1.\lambda_2 = 1 \rightarrow \lambda_1 = \lambda \text{ and } \lambda_2 = 1/\lambda \\ & Tr(\phi) = \lambda_1 + \lambda_2 = \lambda + 1/\lambda \end{aligned}$$

which summarizes into the unique equation :

$$\lambda^2 - Tr(\phi).\lambda + 1 = 0 \tag{2.3}$$

whose roots are Floquet multipliers such that $\lambda_1 = \frac{Tr(\phi) - \sqrt{\Delta}}{2}$ and $\lambda_2 = \frac{1}{\lambda_1}$ [4,4,6].

One can see that Floquet multipliers then only depend on ϕ whose modulation is made through (E, T_{ON}). Therefore, one states the couple (E, T_{ON}) he wants to work with and check if associated Floquet multipliers fulfill $|\lambda_i| < 1$. We will then be able to test values of E and T_{ON} and see which one results into a stable dynamic motion. The point will eventually be to compare results from theory to experimental data.

2.3.1 Theoretical dynamic stability

We apply condition on Floquet multipliers λ_i for each tested couples (10^6 here) and one eventually reaches following analytical graphs showing system's dynamic stability as a function of our parameters (E, T_{ON}), for both damped and non-damped cases :

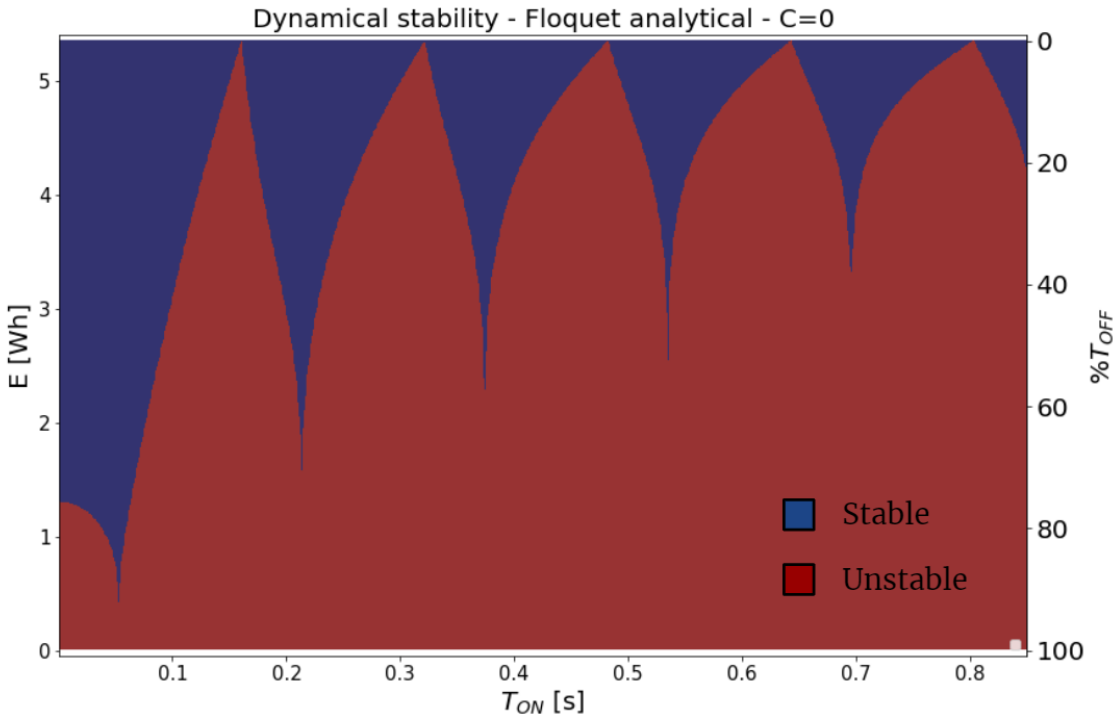

Figure 2.4: Floquet analytical theory - non damped

We here decided to reduce Floquet theory to the study of instability and stability, which implies we applied a binary condition such that the IP is either dynamically stable (0) or unstable (1), thus resulting in only two colors in figure (2.4). The point is to have the same approach than exp measurements : as we didn't look at instability and stability's intensity, we here as well only look at the overall stability state.

On this first graph, we observe 6 instability tongues that develop the same way they did for experimental data, namely we are more unstable when we use less energy to maintain IP up dynamically.

In fact, the one at the very left is in the framework where KAPITZA modulated stability. Therefore, the states to the right are the ones where the driving period is of same order than the collapsing time. We confirm that the electro-magnet allows to extend KAPITZA's stabilisation's framework and we furthermore confirm that the parameters (E, T_{ON}) can lead to the dynamic study of IP's stability.

Besides, figure (2.4) has been confirmed by the numerical Floquet theory, ran for the same E and T_{ON} parameters, furthermore confirming that the analytical graph and our approach make sense regarding the study of IP's dynamical motion.

The point will later on be to compare these analytical theoretical data with experimental ones. Before we do so, let's see the damped case :

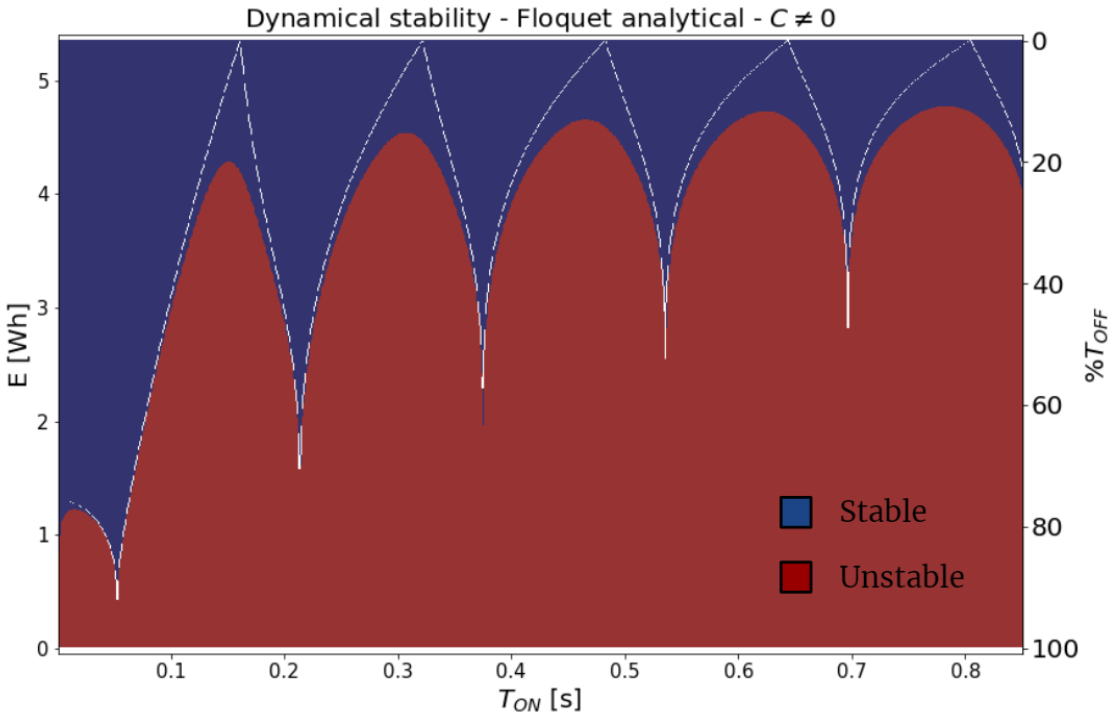

Figure 2.5: Floquet analytical theory - damped

In dashed white line we have where was the non-damped case, while the rest of figure (2.5) corresponds to the damped dynamic motion's stability.

One can see that to consider damping or not doesn't influence the instability tongues' position. It only influences their shapes as instability first occurs for a lower energy E. In fact, it implies that the system is more stable when damped. It translates the fact damping helps lowering oscillation and slows instabilities occurrence.

In our case, with experimental measures, it's this damping effect that made possible the apparition of the forementioned in-between zone where IP continuously oscillates due to a mix of instability behavior and damped vibration.

To study theory when $C \neq 0$ is of a great matter given we based our experimental work under this assumption. We furthermore note that this graph as well has been confirmed by numerical theory.

Let's now compare the analytical results to experimental data.

2.3.2 Comparison experimentation/theory

In this section, we compare our experimental data on dynamic stability (2.2) to analytical results (2.4). We decide to run the comparison with the non-damped case:

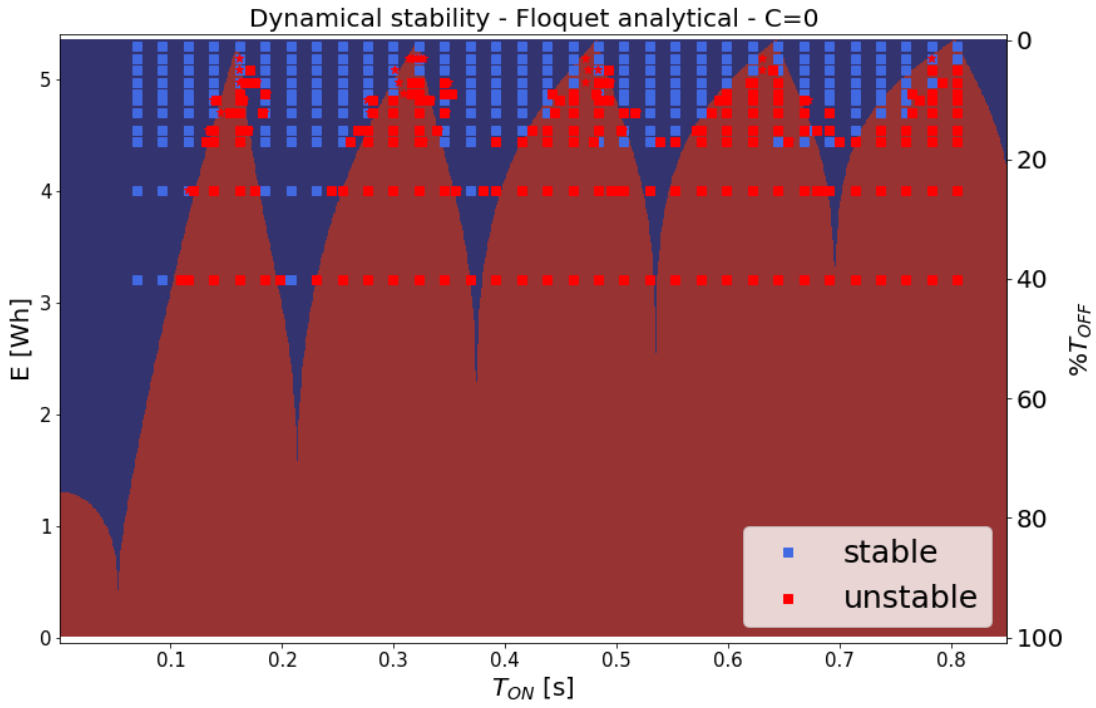

Figure 2.6: Floquet analytical theory - damped

Figure (2.6) shows that experimentation and theory fit well regarding instability and stability occurrences, which gives credit to our experimental measures for both stable and unstable states. Therefore, our experimental protocol is adapted to the study of dynamic stability.

However, one can see we fit the non-damped theory while we rather should fit the damped one. Indeed, we based our empirical models in part on equation (1.1), and so we have a contradiction.

Among our experimental protocol, this can be explained by the impulse step. During this step, we force IP's initial movement to prevent the influence of friction. Yet, doing so, we may remove inertia term such that IP moves directly and doesn't has to put itself in movement. What this observation tells us is that :

- either the impulse we give is too high, thus removing the inertia force component ;
- or maybe what we thought was friction was in fact the setting in movement that was delaying instability apparition.

In both cases, the quantitative study of friction would be useful to have some hindsight on IP's motion and stability. We didn't do it during this report but this observation on damping's influence is a starting point for who may continue the study.

On our hand, we now know experimental data conclude on the existence of dynamical stability. What is left to do is to deduce a theoretical model that tells us where optimal stability occurs.

2.4 Energy optimization

We conclude this report with the model of energy optimization in dynamic stability. In the next few sections, we will explain how one reached the following equation of optimal period :

$$T_{opt}(\equiv T_{ON}) = m \times T_\omega + b(i) \tag{2.4}$$

as well the graph showing stable and unstable periods of modulation:

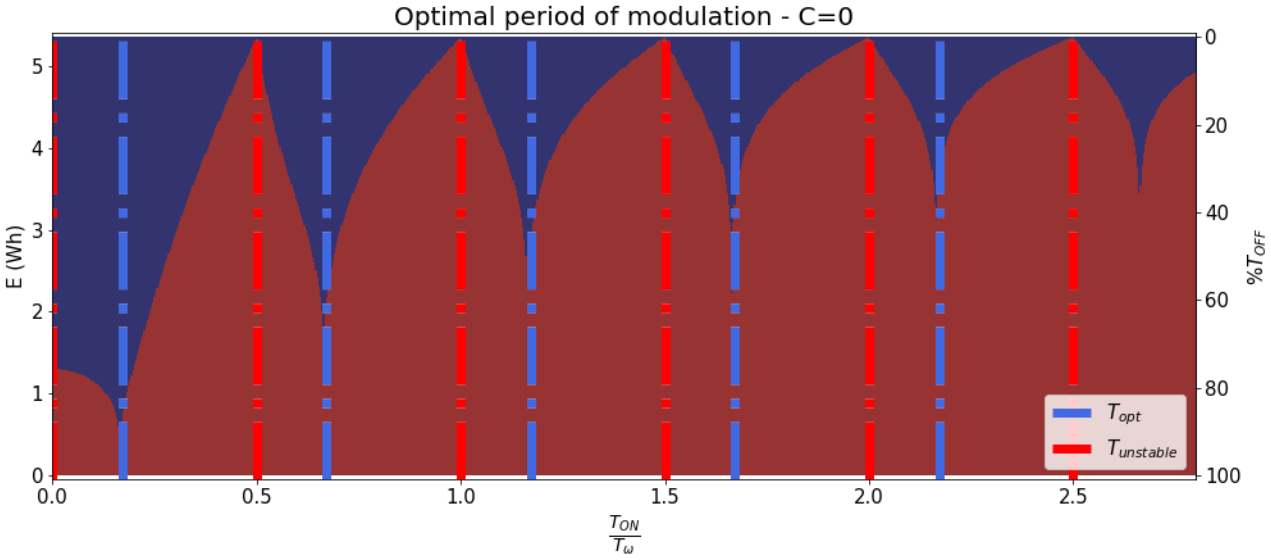

Figure 2.7: Stable/Unstable periods of modulation

a. Instability tongues occurrence

On above graph (2.7) one can see instability tongues (red lines) occur every:

$$T_{res}(\equiv T_{ON}) = \frac{k}{2} \times T_\omega \tag{2.5}$$

with k the number of the tongue and T_ω the period associated to pulsation ω such that $T_\omega = \frac{2\pi}{\omega}$. This time is a characteristic time that is ruling the parametric resonance behind instability tongues. Indeed, when electro-magnet is ON, T_ω is the IP's period of vibration. We thus deduced it might impact the system's behavior, as a parametric resonance parameter.

The point with understanding where are unstable modulation periods (i.e. T_{ON}) is that a similar scheme for stable modulation periods may exist. Before we check this point, let's give some physical sense to equation (2.5).

b. T_{res}'s shape

The equation (2.5) indicates a periodic occurrence of instability tongues, in link with the characteristic time T_ω. Yet, the term $\frac{k}{2}$ as well indicates a characteristic term which is directly bounded to the tongues.

In fact, each tongue is characterized by a certain number of oscillation the IP does in a modulation period. Let's explain that through the instability tongues experimentally observed:

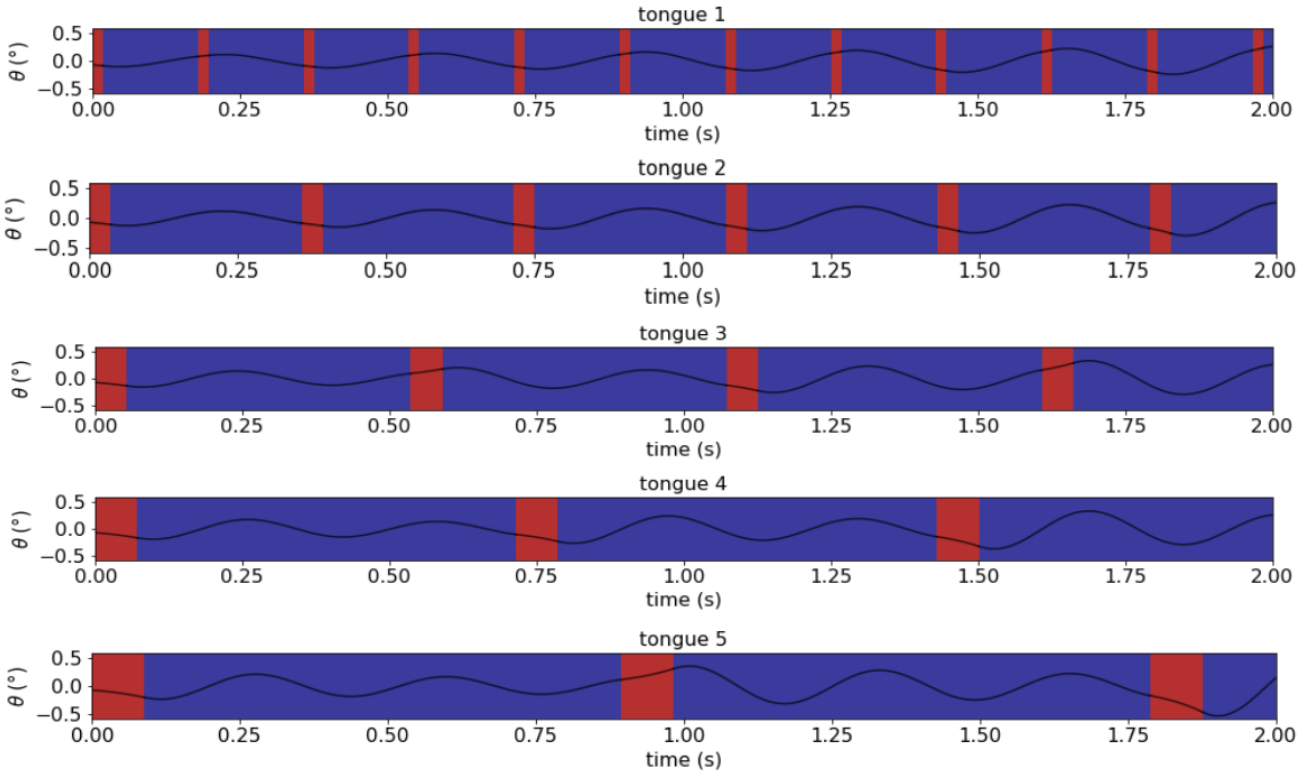

Figure 2.8: Illustration instability behavior for $E = 0.9E_0$

We have on figure (2.8) the shape of IP's motion at each of the 5 instability tongues we observed experimentally (2.6).

Depending on the tongue we are at, IP does more or less oscillations : the bigger T_{res}, the more oscillations IP does during a period of modulation. In details during a modulation period:

- for tongue 1 : IP does half an oscillation and $T_{ON} = \frac{1}{2} \times T_\omega$;
- for tongue 2 : IP does one oscillation and $T_{ON} = \frac{2}{2} \times T_\omega$;
- for tongue 3 : IP does one and a half oscillation and $T_{ON} = \frac{3}{2} \times T_\omega$;
- etc

We can then see the term $\frac{k}{2}$ as the number of oscillations the IP does during one modulation period.

We deduce

$$T_{res} = m \times T_\omega \tag{2.6}$$

with m the number of oscillation IP does in one period of modulation. This last expression then summarizes the IP instability occurrence into a very simple equation.

Moreover, as $\omega = \omega(i)$ we have subsequently that $T_\omega = \frac{2\pi}{\omega(i)} = T_\omega(i)$ such that knowing i one can directly tell where instability is gonna occur. Similarly, we will derive the same kind of equation for the stable case.

Let's conclude on the optimal period of modulation T_{ON} where energy is minimized.

c. Optimal period of modulation

Referring to figure (2.7), blue lines represent the modulation periods where dynamic stability is optimized with respect to energy. One then want to know the modulation period T_{ON} at which this occurs.

The simplest form one may think for T_{opt} is to consider T_{res} equation, with an offset in time, namely :

$$T_{opt} = T_{res} + b$$

with b an offset in time. We then looked for b under a polynomial form given the shape of T_{res} : we know that $T_{res} = m \times T_\omega = \frac{2\pi m}{\omega(i)} = \frac{2\pi m}{\alpha_1 \times i + \beta_1}$ with $(\alpha_1, \beta_1) \in \mathbb{R}$. In the end, we found after numerical interpolation that b may be written under the polynomial form :

$$b(i) = \frac{1}{\alpha_2 i^2 + \beta_2 i + \gamma_2}$$

with $(\alpha_2, \beta_2, \gamma_2) \in \mathbb{R}$ (see Appendix B Fig 3 - factor b calculation for the details on the numerical interpolation and b's shape). The physical meaning of this b term has not been found during this report and so it must be furthermore explored to fully understand the dynamical stability of an inverted pendulum.

Eventually, we deduced from analytical theory an equation for the optimal period of modulation where IP is dynamically stable:

$$T_{opt} = m \times T_\omega + b(i) \tag{2.7}$$

Equation (2.7) defines the theoretical model concluding our work on IP study.

Let's now conclude on this report by going through practical applications one may consider for the work done here.

Conclusion

We went from an unstable system to first a static and then a dynamic stabilization.

This report showed that modulating the stability of the inverted pendulum through an electro-magnet enabled to reach dynamic stable states where the driving frequency was of same order than the collapsing time. We then modulated stability through 2 parameters : the modulation period T_{ON} and the energy E.

We furthermore deduced a theoretical model that provides values for optimal modulation periods T_{ON}, where energy E is minimized.

Finally, with the generalization work achieved so far, we can extend our study to other models and frameworks. Some modifications will however be necessary to reach wider frameworks, ensure a natural divergence, etc.

In some extent, the work done here can be used on most vibrating system whose interacting with their environment may lead to parametric resonance ; as well as more practical subjects as in aerodynamic flutter [7].

A. Appendice A - detail calculation

A.1 Relative error calculation

The error calculated here is the one associated to the one of rod's mass :

$$m = \rho_{plexi} \times V_{rod}$$

the rod being made of plexiglass.

It leads to :

$$\Delta m = m \times \left(\frac{\Delta \rho}{\rho} + \frac{\Delta V}{V} \right)$$

Yet,

$$\Delta V = V \times \left(\frac{\Delta L}{L} + \frac{\Delta l}{l} + \frac{\Delta e}{e} \right)$$

Such that :

$$\Delta m = m \times \left(\frac{\Delta \rho}{\rho} + \frac{\Delta L}{L} + \frac{\Delta l}{l} + \frac{\Delta e}{e} \right) = 1.53 * 10^{-3} \left(\frac{10}{1180} + \frac{0.2}{52} + \frac{0.2}{5} + \frac{0.2}{5} \right) \approx \mathbf{0.14} \text{ g}$$

A.2 Oscillation equation

We will develop the equation defining motion of the inverted pendulum. First and foremost, we use 1.2 figure and the variables, forces, etc detailed on it to do the equation.

Using Lagrange method :

$$\frac{d}{dt} \left(\frac{\partial L}{\partial \dot{q}} \right) - \frac{\partial L}{\partial q} + \frac{\partial D}{\partial \dot{q}} = Q$$

with $D = \frac{1}{2} C \dot{\theta}^2$ the friction term, Q the term of generalized forces, and L the Lagrangian, with $L = T - U$, T the kinetic energy and U the potential energy.

We here go from an equilibrium of the forces and derive an equation for IP.

A.2.1 L calculation

T formula

We then have :

$$T = \frac{1}{2} \left\{ \begin{matrix} \underline{\Omega}(S/\mathbb{R}) \\ \underline{v}(C \in S/\mathbb{R}) \end{matrix} \right\} \bigotimes \left\{ \begin{matrix} \underline{p}(S/\mathbb{R}) \\ \underline{\sigma}(C \in S/\mathbb{R}) \end{matrix} \right\} = \frac{1}{2} (\underline{p}.\underline{v} + \underline{\Omega}.\underline{\sigma});$$

It comes, calculating at center of inertia :

$$T = \frac{1}{2}(\underline{p}.\underline{v} + \underline{\Omega}.\underline{\sigma}) = \frac{1}{2}(M||\underline{v}||^2 + I||\underline{\dot{\theta}}||^2);$$

with M the mass of the system, $\underline{v}$ its speed, I the moment of inertia around rotation axis and $\dot{\theta}$ the rotational speed.

Eventually, as we consider 2 elements composing the system (i.e. $marble + rod$), we have :

$$\underline{OG}_{marble} = (L+r)\underline{e_r} \rightarrow \underline{v}_{marble} = -(L+r)\underline{e_\theta}\dot{\theta}$$

$$\underline{OG}_{rod} = \frac{L}{2}\underline{e_r} \rightarrow \underline{v}_{marble} = -\frac{L}{2}\underline{e_\theta}\dot{\theta}$$

such that : $T = \frac{1}{2}(M_{marble}(L+r)^2 + M_{rod}(\frac{L}{2})^2 + I_{Gy})\dot{\theta}^2$

In detail, the term of inertia comes from the product of rotational speed and kinetic moment : $\underline{\Omega}.\underline{\sigma} = \underline{\Omega}.\underline{\underline{J}}(C \in S/\mathbb{R}).[\underline{\Omega}] = \begin{pmatrix} 0 \\ \dot{\theta} \\ 0 \end{pmatrix} . \begin{pmatrix} I_{Gx} & -I_{Gxy} & -I_{Gxz} \\ -I_{Gxy} & I_{Gy} & -I_{Gyz} \\ -I_{Gxz} & -I_{Gyz} & I_{Gz} \end{pmatrix} \begin{bmatrix} 0 \\ \dot{\theta} \\ 0 \end{bmatrix}$

Moment of inertia calculation

Without going to much in the details, by a use of Huygens theorem in part, we have:

$$\underline{\underline{J}}(G_1 \in S_1/\mathbb{R}) = \frac{2}{5}M_{marble}r^2\underline{\underline{\mathbb{1}}}$$

$$\underline{\underline{J}}(G_2 \in S_2/\mathbb{R}) = \frac{1}{12}M_{rod}\begin{pmatrix} e^2+L^2 & 0 & 0 \\ 0 & L^2+l^2 & 0 \\ 0 & -I_{Gyz} & e^2+l^2 \end{pmatrix}$$

with S_1 the marble and S_2 the rod.

Yet, $\underline{OG} = \dfrac{M\underline{OG}_{marble} + m\underline{OG}_{rod}}{M+m} = \dfrac{M(L+r)\underline{e_r} + m\frac{L}{2}\underline{e_r}}{M+m}$. From now on we note $M_{marble} = M$ and $M_{rod} = m$.

Then using Huygens theorem it comes :

$$\underline{\underline{J}}(0 \in S_1/\mathbb{R}) = \underline{\underline{J}}(G_1 \in S_1/\mathbb{R}) + M \times (L+r)^2 \begin{pmatrix} 1 & 0 & 0 \\ 0 & 1 & 0 \\ 0 & 0 & 0 \end{pmatrix}$$

$$\underline{\underline{J}}(0 \in S_2/\mathbb{R}) = \underline{\underline{J}}(G_2 \in S_2/\mathbb{R}) + m \times \left(\frac{L}{2}\right)^2 \begin{pmatrix} 1 & 0 & 0 \\ 0 & 1 & 0 \\ 0 & 0 & 0 \end{pmatrix}$$

Eventually, we get

$$\underline{\underline{J}}(0 \in S/\mathbb{R}) = \underline{\underline{J}}(0 \in S_1/\mathbb{R}) + \underline{\underline{J}}(0 \in S_2/\mathbb{R})$$

$$\underline{\underline{J}}(G \in S/\mathbb{R}) = \underline{\underline{J}}(0 \in S/\mathbb{R}) - (M+m)||\underline{OG}||^2 \begin{pmatrix} 1 & 0 & 0 \\ 0 & 1 & 0 \\ 0 & 0 & 0 \end{pmatrix}$$

with G the center of inertia of entire system : $\{marble + rod\}$. Eventually, $I_{Gy} = \underline{\underline{J}}(G \in S/\mathbb{R})(e_y \otimes e_y)$.

A.2.2 Q calculation

For what is up to the forces, we decided to model every forces as ext. forces, such that they're accounted in generalized force term Q. Then $U = 0$ in this model such that $L = T$. Then :

$$\sum \underline{F}_{ext}.\underline{v} = (\underline{P} + \underline{F}(I))\underline{v} = Q.\dot{q}$$

with $\dot{q}$ the DOF (i.e. $\dot{\theta}$ here).

P being the force of gravity and F(I) the one of the magnetic field from electro-magnet. The point to consider forces in Q is to account for a likely momentum created during movement. We get :

$$\underline{P} + \underline{F}(I) = (-(M+m)g\underline{e_z} + F(I)\underline{e_z}) \times (-||\underline{OG}||.\dot{\theta}sin(\theta)\underline{e_z}) = Q.\dot{\theta}$$

By identification, it finally comes that :

$$Q = ((M+m)g - F(I)) \times ||\underline{OG}||.sin(\theta)$$

A.2.3 Movement equation

Now that all terms are known, we combine them into Lagrange equation:

$$((M+m)||\underline{OG}||^2 + I_{Gy}) \times \ddot{\theta} + C \times \dot{\theta} = ((M+m)g - F(I))||\underline{OG}|| \times sin(\theta)$$

We conclude on the IP movement equation:

$$((M+m)||\underline{OG}||^2 + I_{Gy}) \times \ddot{\theta} + C \times \dot{\theta} + (F(I) - (M+m)g)||\underline{OG}|| \times sin(\theta) = 0$$

B. Appendice B - additional figures

B.1 Fig 1 - error graphs

To conclude on the L_2 error relevance, we must check how different are experimental values from optimal values. Moreover, if there are big differences, we would like to see if it's an error linked to the height and/or to the initial angle θ_0.

We deduced values for ω and ξ in chapter (1.2.1). We thus look at relative errors e_ω and e_ξ respectively. We then do 2 graphs, both containing the 12 experimental points :

- one that sorts points as a function of θ_0 ;
- the other one that sorts point as a function of h.

It comes :

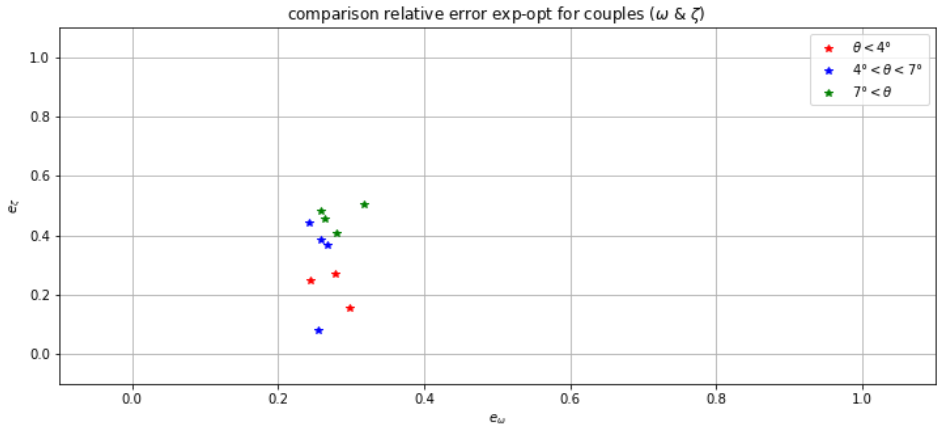

Figure B.1: Relative error exp vs opt values as a function of θ_0

Figure B.2: Relative error exp vs opt values as a function of h

We observe that :

- the relative error on ω : $e_\omega \approx 25\%$ such that $\omega_{exp} = \omega_{opti} \pm 0.25 * \omega_{opti}$;
- the relative error on ω looks to be constant over h and θ_0 such that it may rather be linked to an experimental error than a dependence on parameters (h, θ_0);
- the error on ξ doesn't depend on h while it changes with θ_0. We get that bigger $\theta \gg 1°$, bigger the error on the damping coefficient.
- for ξ as well the relative error $e_\xi \approx 20\%$ for range $\theta \in [2, 6]°$, which is acceptable.

The relative errors are acceptable but they reveal one must limit the framework we work at to ensure the relative error is minimal. We thus deduce we must have $\theta_0 \lesssim 6°$.

B.2 Fig 2 - resistance calculation

In this section, we develop the experimental calculation of the resistance R. The point is that from experimental observation, IP's characteristics depend on the heat we work at.

Indeed, there are losses of energy under heat form. It directly impacts the resistance R. Let's quantify this :

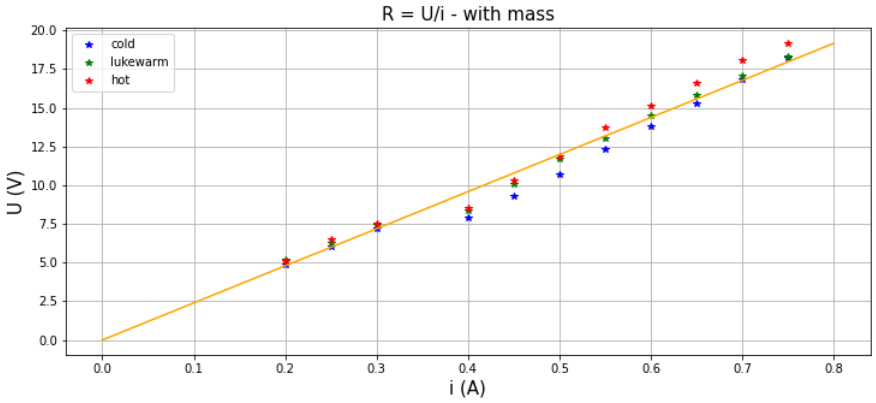

Figure B.3: Illustration modes at $E = 0.9E_0$

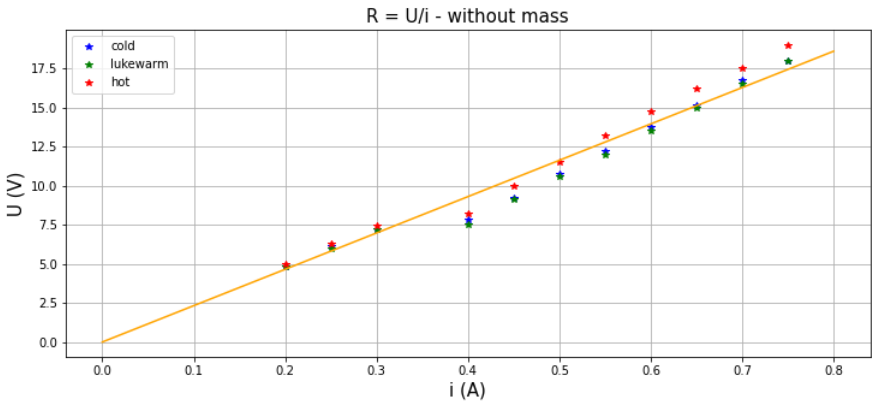

Figure B.4: Illustration modes at $E = 0.9E_0$

We note that the slope of graph U as a function of i is resistance R. We can see a slight change in its value in function of electro-magnet's heat. The condition of heat is being judged by hand but its identification isn't user related.

We as well tested the presence of a mass below magnet and we see it doesn't influence the values of R.

In the end, the value we considered for R is the one from B.3, from orange line which is an empirical model.

B.3 Fig 3 - factor b calculation

In this last section, we show the graph associated to equation

$$b(i) = \frac{1}{\alpha i^2 + \beta i + \gamma}$$

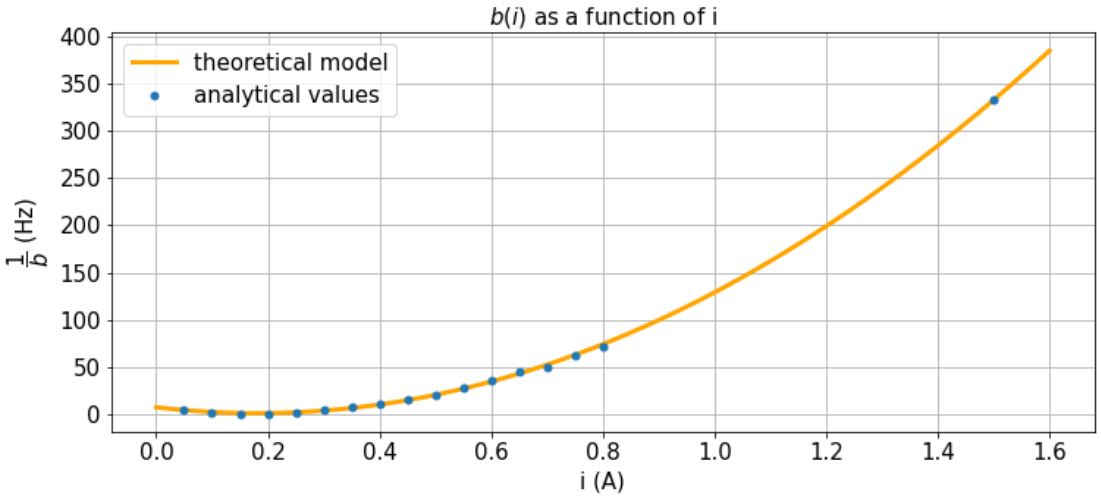

Figure B.5: Illustration modes at $E = 0.9E_0$

As $\frac{1}{b(i)}$ is an order 2 polynomial, we do have $b(i) = \frac{1}{\alpha i^2 + \beta i + \gamma}$. This theoretical model must be furthermore developed to understand the physic behind it.

References

[1] E. Butikov. Kapitza pendulum : A physically transparent simple explanation. 2017.

[2] E. Antonin A. Benjamin, N. Filip F. Emmanuel. Floating under a levitating liquid. *ESPCI Paris, Sorbonne University.*

[3] L. Arnaud G. Alvaro, P. Suzie. Enhancing and controlling parametric instabilities in mechanical systems. *Extreme Mechanics Letters, Elsevier*, 43, 2021.

[4] R. Luppes E. Folkers, A.E. Sterk. Floquet's theorem. Bachelor's project mathematics, University of groningen, faculty of science, mathematics and applied mathematics, July 2018.

[5] A.H. Fatimah. Floquet theory on banach space. Master's thesis, University of groningen, faculty of science, mathematics and applied mathematics, 2013.

[6] F. Sadyrbaev A. Baryshnikov. Remark on the meissner problem. *Proceedings of IMCS of University of Latvia*, 14:1–4, 2014.

[7] B Sun X Zhang. Parametric study on the aerodynamic stability of a long-span suspension bridge. *Journal of Wind Engineering and Industrial Aerodynamics*, 92:431–439, 2004.